Pflügers Arch - Eur J Physiol (2002) 444:99–106
DOI 10.1007/s00424-002-0804-2

ORIGINAL ARTICLE

Joseph Santos-Sacchi · Enrique Navarrete

Voltage-dependent changes in specific membrane capacitance caused by prestin, the outer hair cell lateral membrane motor

Received: 4 December 2001 / Revised: 23 January 2002 / Accepted: 23 January 2002 / Published online: 20 February 2002

Abstract In the outer hair cell (OHC), membrane capacitance principally derives from two components – that associated with lateral membrane sensor/motor charge movement, and that proportional to the membrane surface area (C_{sa}). We used measures of membrane capacitance to test a model hypothesis that OHC lateral membrane molecular motors, recently identified as the protein prestin, fluctuate between two area states. By measuring membrane capacitance in native OHCs or prestin-transfected HEK cells at extreme voltages (±200 mV) where motor-derived charge movement is small or absent, we observed that C_{sa} depends on the state of the motors, or correspondingly on membrane voltage. Deiters cells or control HEK cells, which lack motors, do not show this dependence. We modeled the voltage-dependent change in C_{sa} as a Boltzmann process with the same parameters that describe the charge movement of the motors' voltage sensors. C_{sa} is 3.28±0.75 pF (mean ±SD; n=23) larger during extreme hyperpolarization, and the number of motors in OHCs and prestin-transfected HEK cells correlates with the magnitude of ΔC_{sa} (r=0.78). Although these data are consistent with the area motor model, the corresponding area change, assuming 0.5 μF/cm^2 under constant membrane thickness, is unphysiologically large, and indicates that the capacitance change must result from changes not only in lateral membrane area but also specific capacitance. Thus, we conclude that a conformational change in the lateral membrane motor, prestin, additionally alters the dielectric constant and/or thickness of the lateral plasma membrane.

Keywords Gating charge · Membrane capacitance · Motility

J. Santos-Sacchi (✉) · E. Navarrete
Sections of Otolaryngology and Neurobiology, Yale University School of Medicine, 333 Cedar St., New Haven, CT 06510 USA
e-mail: joseph.santos-sacchi@yale.edu
Tel.: +1-203-7857566 office, Fax: +1-203-7372502

Introduction

The capacitance per unit area of plasma membrane, i.e., specific capacitance (C_{sp}), is determined by the membrane's dielectric constant and thickness. It is a robust quantity that Cole [5] described as "largely independent of cell physiology, pathology and pharmacology, and probably life itself". Based on this property, the magnitude of an individual cell's membrane capacitance (C_m=surface area × C_{sp}) may be considered fixed, invariant with changes in membrane voltage. In that same essay, however, Cole realized that his view could be modified by future investigations; it is now known that deviations from the expected invariant behavior provide information on such varied processes as ionic channel gating [10], synaptic vesicle fusion [29], gap junctional coupling [36], and, in the case of the outer hair cell (OHC), its lateral membrane motor's activity [2, 37]. In the OHC, such deviation arises from restricted charge movement during conformational change in a membrane motor protein [2, 37], the recently identified lateral membrane protein, prestin [26, 41, 48]. Consequently, membrane capacitance (C_m) in the OHC is characterized as a bell-shaped, voltage-dependent capacitance (C_v) that rides atop a parallel capacitance (C_{sa}) whose magnitude is proportional to cell surface area [2, 16, 37]. Peak motor-associated capacitance can range up to nearly twice that of the cell's C_{sa} [39].

One of the model mechanisms whereby the lateral membrane motor can effect whole-cell mechanical responses is by changing the surface area that it occupies within the lateral plasma membrane [17, 18, 38], although other models have been proposed [7, 14, 22, 33]. We reasoned that if the integral lateral membrane motors fluctuate in area between two states, as the model suggests, we should be able to observe whole-cell changes in C_{sa} due to changes in the cell's surface area. Indeed, one of the major criticisms of the area-motor model has been the apparent absence of effects on C_{sa} [33]. According to the model, depolarization, which is predicted to drive the motors into the compact state and reduce the

area occupied by them within the bilayer, should in turn reduce total membrane surface area and C_{sa}, whereas hyperpolarization should do the opposite. In order to test this prediction, we measured capacitance over an extreme voltage range in isolated OHCs and prestin-transfected human embryonic kidney cells under whole-cell voltage-clamp conditions. At extreme voltage polarities where motor-derived charge movement is small or absent, we find that C_{sa} depends on the state of the motors, or correspondingly on membrane voltage. During extreme hyperpolarization, when the motors cause the cylindrical OHC to elongate, C_{sa} is increased – a prediction of the area motor model of OHC motility [17, 18, 38]. Nevertheless, the predicted area change based on typical, fixed values of specific membrane capacitance is unphysiologically large, and must be accounted for by additional mechanisms such as membrane thinning or alterations in the membrane's dielectric properties.

Materials and methods

Guinea pigs were decapitated following anesthetic overdose with halothane, in accordance with the guidelines of Yale University's Animal Care and Use Committee. OHCs were freshly isolated from the guinea pig cochlea using dispase (1 mg/ml) followed by trituration. Transient transfection of human embryonic kidney (TSA201) cells with gerbil prestin was performed as previously described [48]. Co-expression of green fluorescent protein (GFP) provided visual identification of transfected cells. Only isolated, single HEK cells were studied. Cells were whole-cell voltage clamped at room temperature using an Axon 200B amplifier. Membrane voltages were corrected for the effects of residual series resistance, which ranged from 3–5 MΩ. Ionic blocking solutions were used with all cell types to remove voltage-dependent ionic conductances so that capacitive currents could be analyzed in isolation [37]. Extracellular solution: 100 mM NaCl, 20 mM TEA, 20 mM CsCl, 2 mM $CoCl_2$, 1.48 mM $MgCl_2$, 2 mM $CaCl_2$, 10 mM HEPES, and 5 mM dextrose, adjusted to pH 7.2 with NaOH, and adjusted to 300 mosmol/l with dextrose; in some cases $CaCl_2$ and $MgCl_2$ were omitted. Pipette solution: 140 mM CsCl, 10 mM EGTA, 2 mM $MgCl_2$, and 10 mM HEPES, adjusted to pH 7.2 with CsOH, and adjusted to 300 mosmol/l with dextrose. In some experiments, the extracellular solution was also used in patch electrodes. For experiments with 10 mM sodium salicylate, NaCl was reduced to maintain osmolarity. In a few experiments, 50 µM $GdCl_3$ was included in the extracellular solution to decrease residual currents. At this concentration, gadolinium has an insignificant effect on OHC capacitance [21]. Capacitance was measured with a continuous high-resolution (2.56 ms) two-sine voltage stimulus protocol (20 mV peak at both 390.6 and 781.2 Hz), and subsequent FFT-based admittance analysis [40], utilizing the parameter derivations provided by Pusch and Neher [32]. These small, high-frequency sinusoids were superimposed on voltage sinusoids that spanned ±200 mV. OHCs that showed evidence of instability at the extremes were not included (see Results). All data collection and most analyses were performed with an in-house-developed Window's based whole-cell voltage-clamp program, jClamp (SciSoft, CT), utilizing either an Axon Instruments Digidata 1320 board or a National Instruments PCI-6052E board. Matlab (Natick, Mass., USA) was used for fitting the capacitance data. Fits were made with the Nelder-Meade algorithm, and the minimization metric employed was $s=\Sigma\sqrt{[(C_m-\text{fit})^2]}$. In some cases, we used Sigmaplot (Jandel Scientific, California, USA) to fit model data, and determine standard errors.

Results

Under whole-cell voltage-clamp, OHCs do not tolerate extreme voltages that are abrupt in onset. We have only been able to record consistently from cells using a low-frequency sinusoidal stimulus whose range was limited to ±200 mV (not including the superimposed high frequency two-sine stimuli – see Materials and methods). Whole-cell voltages more extreme than that usually resulted in loss of recordings. In a separate study we determined that breakdown in the membranes of the OHC oc-

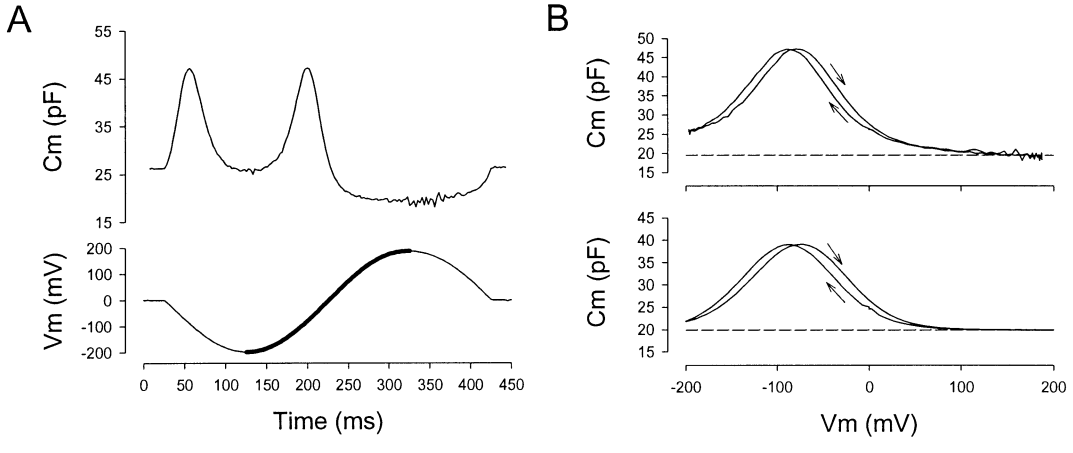

Fig. 1A, B Outer hair cell (*OHC*) capacitance shows hysteresis and asymmetry at voltage polarity extremes. **A** Stimulation with a wide-ranging voltage sinusoid reveals a voltage-dependent capacitance. The highlighted portion of the voltage stimulus and associated capacitance are used in subsequent fits of the membrane capacitance (C_m) data as in Fig. 3. **B** *Top panel:* C_m versus voltage function from **A**. Note hysteresis. Direction of voltage change is show by *arrows*. Additionally, note that the function is asymmetrical, with C_m at the hyperpolarized extreme never approaching the value of membrane surface area (C_{sa}) found at depolarized potentials. This is more rigorously shown in the fits of Fig. 3. *Dashed line* shows minimum capacitance at depolarized levels. *Lower panel:* model results using the wide-ranging voltage sinusoid (based on model fully described in Santos-Sacchi et al. [40]). *Dashed line* shows minimum capacitance at depolarized levels. The result indicates that the hysteresis is due to dependency on prior voltage, but the asymmetry is not, since model C_{sa} at hyperpolarized levels eventually reaches the same minimum magnitude as at depolarized levels

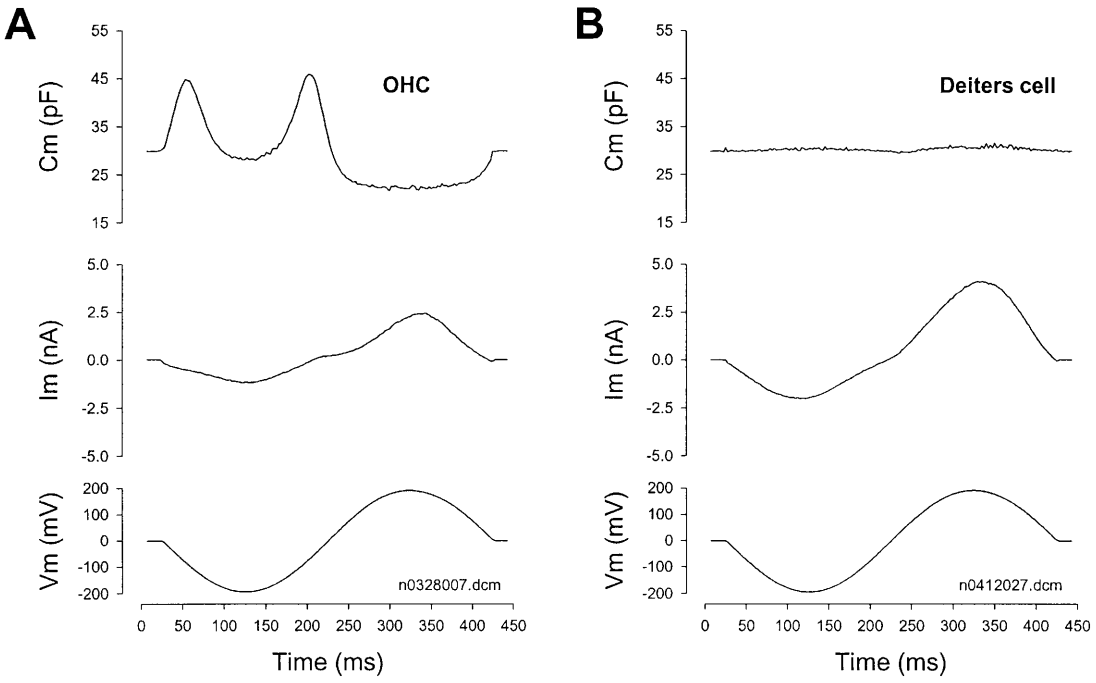

Fig. 2A, B Residual nonlinear current does not influence capacitance measures. **A** Residual nonlinear currents are evoked in the OHC despite our attempts to block membrane conductances. Note that this does not influence the measurement of capacitance, since similar though larger current nonlinearities generated in Deiters' cells (**B**) do not compromise the measurement of its voltage-independent capacitance

curs at absolute membrane potentials greater than 380 mV [27], far greater than the voltage extremes used here; thus, the loss of cells that we experienced with voltages above 200 mV under whole-cell conditions was probably due to compromised pipette-membrane seals resulting from robust mechanical activity of the OHC. We found that deflating the OHC by applying negative pipette pressure, which is known to abolish OHC motility [37], decreased the chances of loss. The results we report here were not affected by reducing OHC turgor pressure. Figure 1A illustrates the membrane capacitance changes that occur with our type of stimulation. During the hyperpolarizing phase of the stimulus, membrane capacitance presents as a double peaked response, and during the depolarizing phase a monophasic minimum is reached. A plot of membrane capacitance (C_m) versus membrane voltage (Fig. 1B, upper panel) shows the bell-shaped capacitance function characteristic of OHCs. However, in this case, two previously unobserved features are found. First, C_m shows hysteresis; namely, C_m magnitude depends on the prior voltage value and, thus, on the direction of voltage change. Second, the bell-shaped C_m function is asymmetrical, indicating that C_{sa} at extreme hyperpolarizations is larger than at extreme depolarizations. The hysteresis is fully predictable since it is known that there is a voltage-dependent shift in the capacitance function that is adequately modeled as a voltage-dependent, motor-induced change in membrane tension [40, 41]. Membrane tension effectively shifts the capacitance function along the voltage axis [11, 17, 20, 47]. Fig. 1B (lower panel) shows the result of that model simulation using our extreme sinusoidal voltage stimulus. The hysteresis is similar to the biophysical data. However, whereas the model output indicates that hysteresis results from voltage-induced shifts in the C_v function, it cannot produce and therefore cannot account for the asymmetry in the C_m function. Additionally, the asymmetry was not related to the initial direction of voltage change, i.e., it did not matter whether the large sinusoid's phase was initially hyperpolarizing (as presented in the figures) or depolarizing. Rate of voltage change was also not influential, as sinusoids from 200 to 800 ms in duration produced the same asymmetry.

Despite the use of ionic blocking solutions, substantial currents are evoked by our extreme voltage protocol (Fig. 2). In order to assure ourselves that large currents or residual current nonlinearities did not confound our measurements, we compared OHC responses to those of supporting Deiters' cells, which lack membrane motors. In Fig. 2 we plot C_m, I_m, and V_m of a typical OHC and typical Deiters' cell. In each case, nonlinear currents are evidenced, notably larger in the Deiters' cell. Yet, Deiters' cells present a linear capacitance largely independent of variations in membrane voltage and current. These control experiments show that unblocked currents do not influence our capacitance measurements. Additionally, we have preliminary data [35] indicating that even in the presence of intracellular and extracellular solutions containing only large impermeant ions, where residual currents are less than 100 pA, capacitance remains asymmetrical. Furthermore, prestin-transfected HEK cells, which display small linear currents, show similar capacitance functions as OHCs (see below). Thus, residual currents and corresponding changes in membrane resistance can-

not account for our C_m data. We also ruled out potential increases of membrane surface area via incorporation of intracellular membrane by recording with high-BAPTA (10–20 mM) or pronase-containing (500 µg/ml) intracellular solutions, treatments known to block membrane fusion [16, 43]. Under these conditions C_{sa} asymmetry is still observed. As an additional check on our admittance technique, we used a standard stair step, transient analysis protocol to confirm the admittance measures within individual OHCs [16]. Although we were unable to provide such extreme voltages as the sinusoidal stimulus because of cell loss, capacitance values measured within the fairly wide range of –160 to 100 mV overlie the admittance-based values (data not shown). We conclude that the asymmetry evidenced in the OHC C_m is real. This asymmetry is illustrated more rigorously through fits of the C_m data.

In order to gauge the asymmetry in our C_m data, we fit the data to the first derivative of a two-state Boltzmann function that has been used routinely to fit OHC C_m data [12, 17, 37].

$$\begin{aligned} C_m &= C_v + C_{sa} \\ C_m &= Q_{max}\frac{ze}{kT}\frac{b}{(1+b)^2} + C_{sa} \\ b &= exp\left(\frac{-ze\,(V_m - V_{pkcm})}{kT}\right) \end{aligned} \tag{1}$$

where C_v is the motor's voltage sensor-associated capacitance, C_{sa} is parallel capacitance proportional to membrane surface area, Q_{max} is the maximum nonlinear charge moved, V_{pkcm} is voltage at peak capacitance or half-maximal nonlinear charge transfer, V_m is membrane potential, z is valence, e is electron charge, k is Boltzmann's constant, and T is absolute temperature. Figure 3A, B show, for two different cells, that this symmetrical function does not adequately describe our C_m data, although the equation had proven sufficient previously [12, 17, 37]. In those previous studies, voltage stimulation was substantially more restricted than employed here, typically not extending beyond ±125 mV, and fits were understandably less constrained. In order to obtain a better understanding of our data, a modified equation was developed, where the state of lateral membrane motors contributes to the magnitude of C_{sa}. We reasoned that the contribution of a putative motor area change would be voltage dependent, and that the relationship should follow a sigmoidal two-state Boltzmann function identical to that of the sensor motor's nonlinear charge movement or the cell's mechanical response [37]. Depolarization, which drives the motor into its compact state, should decrease membrane surface area and C_{sa}. Thus, C_{sa} is described as a sigmoidal function

$$C_{sa} = \frac{\Delta C_{sa}}{(1+b^{-1})} + C_0 \tag{2}$$

where C_0 is defined as the capacitance of the membrane when all motors are in their compact state, the minimum membrane capacitance, ΔC_{sa} is the maximum increase in capacitance that occurs when all motors change from compact to expanded state, and b is as above. The residuals in Fig. 3A, B illustrate the goodness of fit of this modified equation to the C_m data; the average sum of the residuals was halved with the fit to the modified equation (s=8.13 pF for the two-state fit; s=3.96 pF for the modified fit). The significantly better fit substantiates our contention that C_{sa} increases during hyperpolarization, and aids in quantifying the magnitude of change. In Fig. 3C, we plot capacitance functions based on averages of the fitted parameters for 23 cells. The difference in C_{sa} between conditions where all motors exist in either the compact or expanded states is 3.28±0.75 pF (mean ±SD;

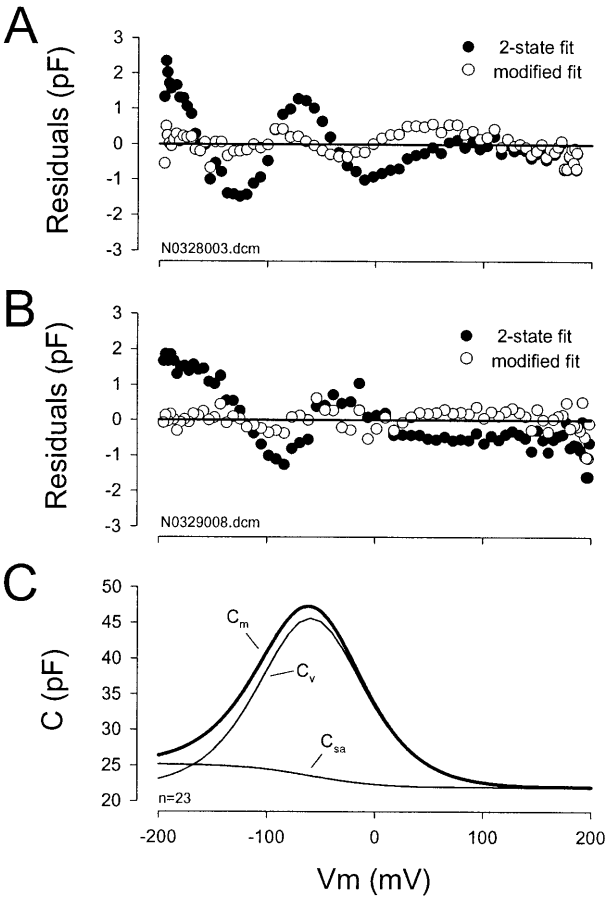

Fig. 3A–C OHCs present two types of voltage-dependent capacitance. **A, B** Plots show residuals of fits to capacitance of two OHCs as a function of membrane voltage. In each case, the C_m data were fit either with an equation based on a simple two-state Boltzmann function (*filled circles*, Eq. 1) or with an additional voltage-dependent C_{sa} component (*open circles*; modified by Eq. 2). Note the poor fit with the simple equation (**A**, *filled circles*: *s*=8.11 pF; **B**, *filled circles*: *s*=8.62 pF), and the good fit with the modified one (**A**, *open circles*: *s*=2.81 pF; **B**, *open circles*: *s*=2.69 pF), especially at negative voltages. **C** OHC capacitance derives from the sum of C_{sa} and C_v to produce C_m. Plots are from fitted parameters of the modified equation for 23 cells (averaged *s*=3.96 pF). Fitted parameters: Q_{max}: 3.09±0.53 pC; V_{pkcm}: –59.4±17.8 mV; z: 0.79±0.10; C_0: 21.9±1.6 pF; ΔC_{sa}: 3.28±0.75 pF. Average residuals for the two-sate fit was *s*=8.13 pF

see Fig. 3C legend for other fitted parameters and statistical comparisons). The plot further illustrates how this voltage-dependent change in C_{sa} results in an asymmetrical C_m function.

Capacitance asymmetry may arise from multi-state models of motor activity; however, Iwasa [19], using realistic values for OHC charge parameters found little evidence of asymmetry in model capacitance functions (his Fig. 3). We also fit our data to the sum of two bell-shaped Boltzmann derivatives, each providing distinct parameters for z, V_{pkcm}, and Q_{max}. In this case however, the fitted parameters of the second underlying Boltzmann are unrealistic; for example, V_{pkcm} is unphysiologically negative in magnitude, showing values as great as –780 mV, with Q_{max} up to 15 pC. Of course, this type of fit describes a function that mimics that of Eq. 2 within the voltage range that we studied.

What evidence is there that ΔC_{sa} results from the activity of OHC lateral membrane motors? This is an important point since recently, Kilic and Lindau [24] have found an asymmetrical bell-shaped membrane capacitance, similar in form to the one we observe here, that they attribute to Na channel gating charge in nerve terminals. In fact, they find voltage-dependent changes in their control C_m recordings (in the absence of Na channel activity) that mimic the form of our Eq. 2. In order to determine whether the activity of the lateral membrane motor accounts for ΔC_{sa}, we measured capacitance in Deiters' cells and HEK cells that were either successfully or unsuccessfully (based on the generation of nonlinear capacitance) transfected with the gene for prestin. Prestin has recently been identified as the OHC motor protein, since when expressed in HEK cells it displays the electro-mechanical signature of the OHC motor [41, 48]. We do not observe voltage-dependent C_m in control cells that lack the motor. Figure 4A shows that Deiters' cells, which lack lateral membrane motors, or human embryonic kidney cells *unsuccessfully* transfected with prestin do not evidence C_m differences at voltage extremes. More telling, those non-auditory cells *successfully* transfected with prestin present asymmetrical capacitance functions matching those of OHCs (Fig. 4B). Additional evidence arises from the direct correlation between the number of membrane motors based on charge estimates ($N=Q_{max}/ze$) and the magnitude of ΔC_{sa} (unconstrained fit, solid line; r=0.78; Fig. 4C). A unit capacitance change of 0.11 aF per motor is obtained. With the fit constrained to the origin (Fig. 4C, dashed line), 0.13 aF per motor is obtained. These data were derived from mature OHCs of different lengths (n=23), from prestin-transfected cells with differing expression efficiencies (n=6), and from published data on developing OHCs (n=2) [30]. Finally, we note that the generation of nonlinear capacitance, in and of itself, is not responsible for the asymmetry we find. That is, treatment with lipophilic ions is able to induce a bell-shaped capacitance in Deiters cells and an augmented capacitance in OHCs. However, we found no evidence that this additional gating charge either produced or augmented the asymmetry

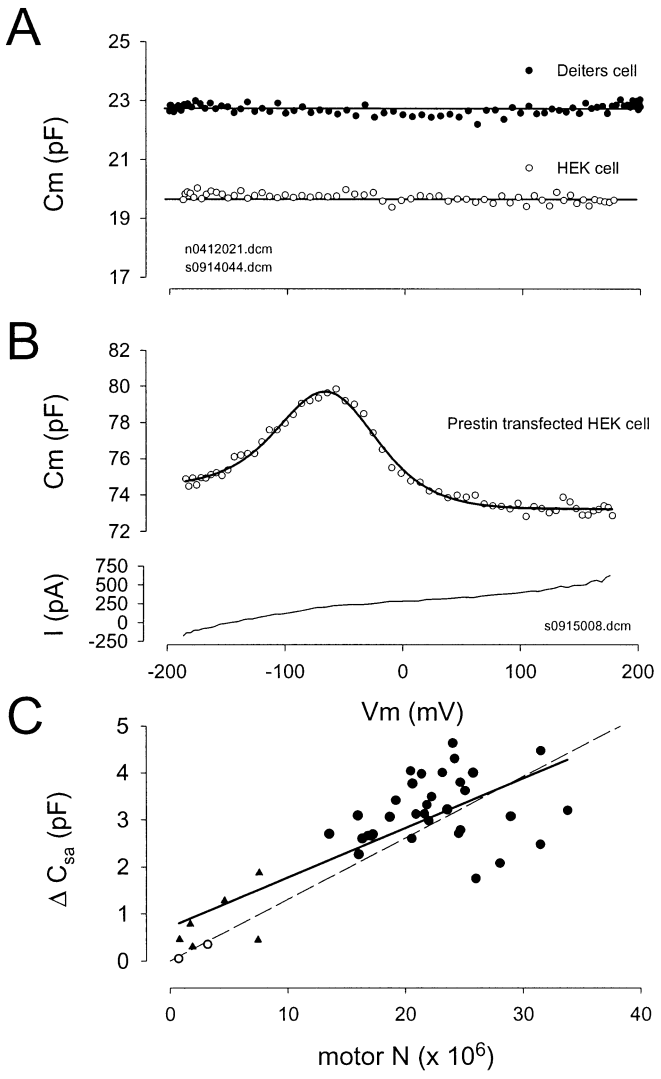

Fig. 4A–C The increase in C_{sa} at hyperpolarized potentials arises from the lateral membrane motor protein, prestin. **A** Neither Deiters' cells (*filled circles*), which do not express prestin, nor human embryonic kidney cell unsuccessfully transfected with prestin (*open circles*) give evidence of an increase in C_{sa} with hyperpolarization. *Lines* are straight horizontals. **B** Prestin-transfected human embryonic kidney cells show the same asymmetrical C_m function as OHCs. *Fitted solid line*: Q_{max}: 0.90 pC; V_{pkcm}: –65.0 mV; z: 0.66; C_0: 73.2 pF; ΔC_{sa}: 1.25 pF. **C** The maximum change in C_{sa} (ΔC_{sa}) is correlated with the estimated number of motors ($N=Q_{max}/ze$). The *filled circles* are adult OHCs, the *filled triangles* are prestin-transfected cells, and the *open circles* are obtained from fits to the developmental OHC data of Oliver and Fakler (their Fig. 1, P6, P11; limited voltage range but low noise traces) [30]. The *dotted line* is a linear regression through the origin (slope of 0.13 aF/motor), whereas the *solid line* is an unconstrained regression, with a slope of 0.11 aF/motor and an r of 0.78

in OHC capacitance [46]. All these data strongly suggest that ΔC_{sa} arises from the activity of lateral membrane motors.

Finally, we explored the effect of the widely used drug, salicylate, on OHC C_{sa}. Salicylate, which can cause temporary hearing loss and tinnitus, has been found to reduce OHC motor-derived capacitance and

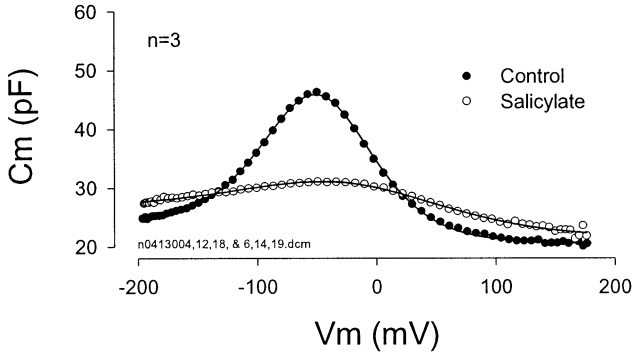

Fig. 5 Salicylate reduces C_v but increases C_{sa}. Averaged responses from three cells before and after extracellular salicylate treatment (10 mM). Three minutes after obtaining the whole-cell configuration control measures were made; following an additional 3 min of superfusion with salicylate the measures were repeated. Note the reduction in motor-derived capacitance, but an increase in C_{sa}. Fitted parameters for control: Q_{max}: 2.93 pC; V_{pkcm}: –48.9 mV; z: 0.83; C_0: 20.5 pF; C_{sa}: 3.6 pF. Fitted parameters for salicylate: Q_{max}: 1.6 pC; V_{pkcm}: –23.2 mV; z: 0.44; C_0: 21.2 pF; C_{sa}: 5.4 pF

motility [21, 42, 44]. Deiters' cell capacitance, on the other hand, is unaltered by salicylate treatments (data not shown). However, the effect on the OHC is not simply to reduce capacitance uniformly across voltage. The averaged data (n=3) in Fig. 5 shows that whereas peak capacitance is substantially reduced, capacitance on either side of the peak actually increases, and this is partially owing to a reduction in the steepness of the voltage dependence, as indicated by the fits to the C_m data (see Fig. 5 legend). Interestingly, the fit with our new model demonstrates that C_{sa} in the hyperpolarized region increases by about 2 pF above controls. Since salicylate has no effect on the capacitance of cells that lack the lateral membrane motor, and since there is a simultaneous effect on C_v and C_{sa}, this result additionally identifies ΔC_{sa} as arising from the activity of lateral membrane motors.

Discussion

In the OHC, membrane capacitance (C_m) arises from two superimposed components; one component (C_v) derives from gating charge movement owing to voltage-dependent activity of motor proteins within the lateral plasma membrane, while the other component (C_{sa}) derives from the intrinsic dielectric properties of all segments of its plasma membrane [2, 8, 37]. The latter component, often termed "linear" membrane capacitance, though typically considered independent of voltage, may co-vary with mechanisms, including voltage-dependent ones, that alter the underlying characteristics which define whole-cell capacitance, namely the membrane's surface area, dielectric constant, or thickness. We find that the activity of the lateral membrane motor, prestin, either in native OHCs or expressed in nonauditory cells influences the magnitude of the plasma membrane's C_{sa}, providing a clue to the motor's mechanism of action.

What fraction of ΔC_{sa} may arise from voltage-induced, OHC lateral membrane area change?

The change in C_{sa} that we observe resulting from fluctuations in the state of lateral membrane motors may arise from corresponding fluctuations in the area occupied by the motors within the lipid bilayer. Direct modifications of membrane surface area by integral proteins can be accomplished by a variety of molecular mechanisms. For example, reversible insertion of proteins or protein regions within the plasma membrane could serve to change membrane surface area [25]. The insertion of the bactericidal colicin protein into the lipid bilayer is voltage dependent, with at least 68 amino acid residues reversibly inserting into the bilayer [23]. Obviously, such a phenomenon will displace lipid, and alter membrane surface area. Alternatively, integral membrane proteins could change surface area by rearrangement of subunits, as may occur in gap junctions [45].

Based on our set of measures, the average number of motors [N=Q_{max}/(ze)] per cell is 25.7±4.3 million. Thus, we estimate that each motor contributes ≅0.13 aF to C_{sa} as the motor changes from the compact to the expanded state. We previously determined the OHC-specific membrane capacitance to be 8 fF/μm^2, accounting for additional membrane area (≅30%; see [6]) due to rippling that is unobservable at the light microscopic level [16]. More recent and rigorous attempts to account for membrane folding provide estimates in other cell types of 5 fF/μm^2 [43]. Using the latter value, we arrive at a motor area change of ≅26 nm^2. Based on our estimates of C_0 (21.9 pF), the area of the lateral membrane can be estimated to be 3134 μm^2, after correcting for the capacitance of those membrane regions devoid of motors (6.23 pF; [16]). The density of motors within the lateral membrane is then 8168/μm^2, similar to our previous estimates obtained from low-frequency OHCs [16, 39]. Given these values, the estimated area change in the lateral membrane, if ΔC_{sa} fully reflects area changes, would be about 21%. This large area change is in contrast with results of modeling. We had previously determined that the OHC area motor model could account for physiological length and diameter changes by a lateral membrane surface area modification of about 3%. Indeed, even the unit motor area change that we now obtain, 26 nm^2, is much larger than estimates previously made (≅8 nm^2 [38]; 2–7 nm^2 [1, 17, 18]; 0.37 nm^2 [11]). We conclude that ΔC_{sa} does not simply reflect changes in the membrane surface area.

Kalinec et al. [22] found voltage-induced surface area changes up to 8% in lateral membrane patches utilizing voltage pulses between ±80 mV. Since this voltage excursion is less than the motor's range of voltage sensitivity, it might be expected that their measured area changes were sub-maximal. Considering the Boltzmann characteristics of the mechanical response [37], their data are reconcilable with a maximal area change of 10.9%. While our capacitance data may be viewed as arising from changes in membrane characteristics other than ar-

ea, the direct measures of Kalinec et al. [22] must be taken at face value and supersede model predictions. It should be noted that the OHC plasma membrane area is not increased by stretch but instead by supplementation; consequently, an area increase above that typically considered to cause membrane breakdown by stretching (≅4%; [9]) is not unrealistic. Thus, we consider that a portion of ΔC_{sa} arises from a 10.9% change in lateral membrane surface area, amounting to 1.7 pF, and the remainder (1.6 pF) reflects changes in either the membrane's dielectric constant or thickness. That is, the specific membrane capacitance changes from 5.0 to 5.37 fF/μm² when all prestin motors change from the compact to the extended state.

How might an integral membrane protein, such as prestin, alter specific membrane capacitance?

Membrane dielectric

The dielectric constant of the lipid bilayer is about 2. Proteins possess a higher dielectric constant, and thus they may be expected to alter the overall dielectric properties of the membrane when inserted within the bilayer. Indeed, many investigators have found changes in capacitance upon insertions of proteins into lipid bilayers, although in some cases the changes were transient [4], or may have been attributed to channel gating capacitance [34]. A direct test with exogenously expressed glycine receptors in HEK cells did not alter the specific membrane capacitance [13], although only about 20,000 receptors were expressed per cell. In the adult OHC from the low-frequency region of the cochlea, 25 million motors are expressed, increasing the likelihood of the protein's effect on the membrane dielectric. Voltage-dependent movement of charged regions of the protein prestin into or out of the hydrophobic membrane domain could affect the membrane dielectric. Alternatively, binding of anions to prestin could change the protein's dielectric [31].

Membrane thickness

Transmembrane voltage may affect membrane thickness directly. Indeed, one of the mechanisms whereby voltage-induced membrane breakdown is thought to occur is via electro-compressive forces [28]. Regardless, it is unlikely that the magnitude of voltages we employed here is capable of inducing sufficient changes in membrane thickness to significantly alter its capacitance, since in control Deiters' and HEK cells, membrane capacitance was not affected by voltage. Interestingly, in pure lipid bilayers, membrane capacitance was shown to be voltage dependent, presumably as a result of membrane compression [3]. Voltage-induced increases in capacitance up to 100% were found. However, those results were attributable to the solvent content of the bilayer. More germane to our data, the action of membrane proteins may also affect bilayer thickness. For example, the anti-microbial peptide, proegrin-1, resides as a membrane surface adsorbed structure (residing within the polar head group region) or as a transmembrane spanning structure [15], depending on the concentration. In the former state, the peptide thins the membrane, whereas in the latter state the membrane is thickened. Little is known about the secondary and tertiary structure of the integral membrane protein prestin, and it may be that some voltage-dependent mechanism akin to the concentration-dependent activity of proegrin-1 is occurring. The possibility cannot be dismissed that the presence of the highly hydrophobic prestin molecule within the lateral membrane provides for an effect similar to the solvent effects observed by Benz and Janko [3]; for example, by altering lipid packing at the protein-lipid interface. In these scenarios, voltage-dependent, prestin-induced perturbations of the bilayer could permit fluctuations of membrane thickness either as a result of the direct compressive action of voltage on a susceptible bilayer or through voltage-induced protein conformational changes. In this regard, salicylate, a drug capable of modifying lipid packing and bilayer mechanics [33], may function to increase the effectiveness of prestin in altering membrane thickness. It should be noted that in either scenario membrane surface area would also change as a function of thickness.

Acknowledgements We thank Margaret Mazzucco for technical help, and Peter Dallos and Fred Sigworth for reading and discussing an early version of the manuscript. This work was supported by NIH-NIDCD grant DC00273 to J.S.S.

References

1. Adachi M, Iwasa KH (1999) Electrically driven motor in the outer hair cell: effect of a mechanical constraint. Proc Natl Acad Sci USA 96:7244–7249
2. Ashmore JF (1990) Forward and reverse transduction in the mammalian cochlea. Neurosci Res Suppl 12:S39–S50
3. Benz R, Janko K (1976) Voltage-induce capacitance relaxation of lipid bilayer membranes. Effects of membrane composition. Biochim Biophys Acta 455:721–738
4. Chanturiya AN (1990) Detection of transient capacitance increase associated with channel formation in lipid bilayers. Biochim Biophys Acta 1026:248–250
5. Cole KS (1971) Some aspects of electrical studies of the squid giant axon membrane. In: Adelman WJ (ed) Biophysics and physiology of excitable membranes. Van Nostrand Reinhold, New York, pp 125–142
6. Dallos P (1983) Some electrical circuit properties of the organ of Corti. I. Analysis without reactive elements. Hear Res 12:89–119
7. Dallos P, Hallworth R, Evans BN (1993) Theory of electrically driven shape changes of cochlear outer hair cells. J Neurophysiol 70:299–323
8. Dong X, Ehrenstein D, Iwasa KH (2000) Fluctuation of motor charge in the lateral membrane of the cochlear outer hair cell. Biophys J 79:1876–1882
9. Evans EA, Waugh R, Melnik L (1976) Elastic area compressibility modulus of red cell membrane. Biophys J 16:585–595
10. Fernandez JM, Bezanilla F, Taylor RE (1982) Distribution and kinetics of membrane dielectric polarization. II. Frequency domain studies of gating currents. J Gen Physiol 79:41–67

11. Gale JE, Ashmore JF (1994) Charge displacement induced by rapid stretch in the basolateral membrane of the guinea-pig outer hair cell. Proc R Soc Lond B Biol Sci 255:243–249
12. Gale JE, Ashmore JF (1997) An intrinsic frequency limit to the cochlear amplifier. Nature 389:63–66
13. Gentet LJ, Stuart GJ, Clements JD (2000) Direct measurement of specific membrane capacitance in neurons. Biophys J 79: 314–320
14. He DZ, Dallos P (1999) Somatic stiffness of cochlear outer hair cells is voltage-dependent. Proc Natl Acad Sci USA 96: 8223–8228
15. Heller WT, Waring AJ, Lehrer RI, Harroun TA, Weiss TM, Yang L, Huang HW (2000) Membrane thinning effect of the beta-sheet antimicrobial protegrin. Biochemistry 39:139–145
16. Huang G, Santos-Sacchi J (1993) Mapping the distribution of the outer hair cell motility voltage sensor by electrical amputation. Biophys J 65:2228–2236
17. Iwasa KH (1993) Effect of stress on the membrane capacitance of the auditory outer hair cell. Biophys J 65:492–498
18. Iwasa KH (1994) A membrane motor model for the fast motility of the outer hair cell. J Acoust Soc Am 96:2216–2224
19. Iwasa KH (1997) Current noise spectrum and capacitance due to the membrane motor of the outer hair cell: theory. Biophys J 73:2965–2971
20. Kakehata S, Santos-Sacchi J (1995) Membrane tension directly shifts voltage dependence of outer hair cell motility and associated gating charge. Biophys J 68:2190–2197
21. Kakehata S, Santos-Sacchi J (1996) Effects of salicylate and lanthanides on outer hair cell motility and associated gating charge. J Neurosci 16:4881–4889
22. Kalinec F, Holley MC, Iwasa KH, Lim DJ, Kachar B (1992) A membrane-based force generation mechanism in auditory sensory cells. Proc Natl Acad Sci USA 89:8671–8675
23. Kienker PK, Qiu X, Slatin SL, Finkelstein A, Jakes KS (1997) Transmembrane insertion of the colicin Ia hydrophobic hairpin. J Membr Biol 157:27–37
24. Kilic G, Lindau M (2001) Voltage-dependent membrane capacitance in rat pituitary nerve terminals due to gating currents. Biophys J 80:1220–1229
25. Lesieur C, Vecsey-Semjen B, Abrami L, Fivaz M, Gisou vdG (1997) Membrane insertion: the strategies of toxins [review]. Mol Membr Biol 14:45–64
26. Ludwig J, Oliver D, Frank G, Klocker N, Gummer AW, Fakler B (2001) Reciprocal electromechanical properties of rat prestin: the motor molecule from rat outer hair cells. Proc Natl Acad Sci USA 98:4178–4183
27. Navarrete E, Santos-Sacchi J (2001) Electropermeabilization and fast resealing in the cellular elements of the mammalian cochlea. Santi, Peter. 24, 72. 2001. St. Petersburg, FL. Assoc Res Otolaryngol Abstract 2-4-2001
28. Needham D, Hochmuth RM (1989) Electro-mechanical permeabilization of lipid vesicles. Role of membrane tension and compressibility. Biophys J 55:1001–1009
29. Neher E, Marty A (1982) Discrete changes of cell membrane capacitance observed under conditions of enhanced secretion in bovine adrenal chromaffin cells. Proc Natl Acad Sci USA 79:6712–6716
30. Oliver D, Fakler B (1999) Expression density and functional characteristics of the outer hair cell motor protein are regulated during postnatal development in rat. J Physiol (Lond) 519:791–800
31. Oliver D, He DZ, Klocker N, Ludwig J, Schulte U, Waldegger S, Ruppersberg JP, Dallos P, Fakler B (2001) Intracellular anions as the voltage sensor of prestin, the outer hair cell motor protein. Science 292:2340–2343
32. Pusch M, Neher E (1988) Rates of diffusional exchange between small cells and a measuring patch pipette. Pflugers Arch 411:204–211
33. Raphael RM, Popel AS, Brownell WE (2000) A membrane bending model of outer hair cell electromotility. Biophys J 78:2844–2862
34. Rojas E, Pollard HB (1987) Membrane capacity measurements suggest a calcium-dependent insertion of synexin into phosphatidylserine bilayers. FEBS Lett 217:25–31
35. Rybalchenko V, Santos-Sacchi J (2001) Modulation of OHC capacitance by Cl^- ions. XXXVIII Workshop on Inner Ear Biology, Rome, Italy. http://ieb.unife.it/ieb2001/roma_index.html
36. Santos-Sacchi J (1991) Isolated supporting cells from the organ of Corti: some whole cell electrical characteristics and estimates of gap junctional conductance. Hear Res 52:89–98
37. Santos-Sacchi J (1991) Reversible inhibition of voltage-dependent outer hair cell motility and capacitance. J Neurosci 11:3096–3110
38. Santos-Sacchi J (1993) Harmonics of outer hair cell motility. Biophys J 65:2217–2227
39. Santos-Sacchi J, Kakehata S, Kikuchi T, Katori Y, Takasaka T (1998) Density of motility-related charge in the outer hair cell of the guinea pig is inversely related to best frequency. Neurosci Lett 256:155–158
40. Santos-Sacchi J, Kakehata S, Takahashi S (1998) Effects of membrane potential on the voltage dependence of motility- related charge in outer hair cells of the guinea-pig. J Physiol (Lond) 510:225–235
41. Santos-Sacchi J, Shen W, Zheng J, Dallos P (2001) Effects of membrane potential and tension on prestin, the outer hair cell lateral membrane motor protein. J Physiol (Lond) 531:661–666
42. Shehata WE, Brownell WE, Dieler R (1991) Effects of salicylate on shape, electromotility and membrane characteristics of isolated outer hair cells from guinea pig cochlea. Acta Otolaryngol (Stockh) 111:707–718
43. Solsona C, Innocenti B, Fernandez JM (1998) Regulation of exocytotic fusion by cell inflation. Biophys J 74:1061–1073
44. Tunstall MJ, Gale JE, Ashmore JF (1995) Action of salicylate on membrane capacitance of outer hair cells from the guinea-pig cochlea. J Physiol (Lond) 485:739–752
45. Unwin N (1989) The structure of ion channels in membranes of excitable cells. Neuron 3:665–676
46. Wu M, Santos-Sacchi J (1998) Effects of lipophilic ions on outer hair cell membrane capacitance and motility. J Membr Biol 166:111–118
47. Zhao HB, Santos-Sacchi J (1999) Auditory collusion and a coupled couple of outer hair cells. Nature 399:359–362
48. Zheng J, Shen W, He DZ, Long KB, Madison LD, Dallos P (2000) Prestin is the motor protein of cochlear outer hair cells. Nature 405:149–155